International Journal for Housing Science and Its Applications
Publish August 4, 2025. Volume 46, Issue 3 Pages 3443-3451

https://doi.org/10.70517/ijhsa463290

Modeling the sensitivity of solar cell current output to environmental changes using time-series data analytics

Jiawei Shen[1], Yuming Xue[1], Luoxin Wang[1,*], Tianen Li[2] and Hongli Dai[1]
[1] Institute of New Energy Intelligence Equipment, Tianjin Key Laboratory of Film Electronic & Communication Devices, School of Integrated Circuit Science and Engineering, Tianjin University of Technology, Tianjin, 300384, China
[2] Institute of Mechanical Engineering, Baoji University of Arts & Science, Baoji, Shaanxi, 721013, China
Corresponding authors: (e-mail: orwellx@tjut.edu.cn).

Abstract Considering the spatial distribution and temporal evolution characteristics of extreme meteorological hazards, this paper constructs a combined model (CNN-LSTM) of convolutional neural network (CNN) and long-short-term memory network (LSTM), and designs the training process of the model. Certain salient features of the environmental change data are captured by the CNN spatial model and these features are used as inputs for constructing the LSTM time series dataset, which reveals the interactions between the hidden features in the data and the space, and thus improves the accuracy of the prediction results. The diffuse reflection coefficient of the solar panel is also calculated as well as the parameters of the model are determined to finalize the environmental change-sensitive nonlinear modeling of the current output characteristics of the solar cell, which is experimentally demonstrated and analyzed. The CNN-LSTM model in this paper outperforms the single LSTM model in the four evaluation indexes of RMSE, MAE, MAPE and R^2 in the training and test sets, and it is able to more accurately capture the small fluctuations of the solar cell current output power in response to the environmental changes, and shows stronger robustness and generalization ability. The reliability and sensitivity of the solar cell are better when the insulating film thickness is 0.2 mm and 0.8 mm, and it has better sensitivity to both temperature and relative humidity, which provides reference information for the sensitivity of solar cell current output to environmental changes using the time series data analysis method.

Index Terms CNN-LSTM model, diffuse reflection coefficient, solar cell, current output characteristics, environmental sensitivity

I. Introduction

With the proposal of “double carbon” goal, various industries have taken various measures to reduce carbon emissions, and the addition of photovoltaic power generation system has become one of the effective methods of green power supply [1], [2]. Photovoltaic power generation system is a new type of power generation system that utilizes the photovoltaic effect of the semiconductor material of solar cells to directly convert solar radiation energy into electrical energy [3]. It has become one of the effective ways of energy supply due to its advantages of cleanliness, environmental protection and wide coverage [4]. However, solar cells are greatly affected by both light intensity and ambient temperature, which are external environmental factors, and the output characteristic curve will change dynamically with time, resulting in the energy conversion efficiency of PV power generation system and environmental changes are closely related [5]-[7]. Among them, low photoelectric conversion efficiency and other issues have become a major constraint on the development of photovoltaic power generation industry [8]. How to ensure the maximum energy conversion of photovoltaic power generation system under the dynamic change of solar light intensity and ambient temperature is the key to realize solar energy as an efficient and reliable energy supply [9], [10]. At the same time, due to the uncertainty and stochastic characteristics of photovoltaic power generation, which is susceptible to the PV surrounding environment, weather, and other factors, the process data collection is also common to the phenomenon of missing data [11]-[13]. Therefore, by collecting multivariate, multidimensional, and large-scale time series data of the current output of PV power generation system, it helps the data subsequent modeling, prediction, and other mining work, and its research work has an important value of popularization and application [14]-[16].

In this paper, the CNN model is used to extract the environmental change spatial feature data of solar cell current output, and then the extracted data features are input into the LSTM model to further deal with the temporal dependence between the data from a higher level. Then the two models were fused to obtain the CNN-LSTM network model, and its design algorithm and construction process were introduced. By capturing information in

different spatial scales and time scales, it is adapted to different complex data patterns. In order to solve the problem of the large difference between the output voltage value and the actual voltage value of the traditional solar cell, the output factor of the solar cell is calculated and the parameters of the model are determined, and the harmonic components are used to assist in the construction of the nonlinear modeling of the output characteristics of the solar cell. Finally, the prediction results of the model are analyzed and the environmental sensitivity of solar cells is studied as an example.

II. CNN-LSTM based solar cell current output model construction

II. A. CNN-LSTM neural network

II. A. 1) CNN networks

CNN is a special class of neural network, very suitable for processing data with spatial structure. CNN can directly accept multi-channel matrix data without element rearrangement, make full use of the spatial properties of the training set, and its as a spatial model is able to extract spatial information from the data in an automatic and hierarchical way. CNN is mainly composed of convolutional layer, pooling layer and activation layer.

(1) Convolutional layer: the most important feature of CNN is the convolutional operation. The convolution layer can maintain the spatial continuity of the input data, detect local patterns in the input data, and can extract the local features of the data. The 2D convolution operation in CNN can be formulated as:

$$X_i^l = X_i^{l-1} \otimes K_i^l + b_i^l \tag{1}$$

where $\otimes$ is the convolution operation; X_i^l is the l th layer feature mapped by the i th convolution kernel, K_i^l; the convolution kernel, $K_i^l \in \square^{C\times H\times W}$, is the three-dimensional weighting tensor, where C is the number of channels, $H\times W$ is the kernel size; X_i^{l-1} is the $l-1$ th layer feature; and b_i^l is the bias.

The convolutional layer essentially performs inter-correlation operations, automatically processing the correlation features between the input data to achieve feature extraction, and gradually mapping the features to the high-dimensional space. Specifically, feature extraction is performed for all grid attributes within the spatial sensing field, thus fully utilizing the adjacent grid information.

(2) Pooling layer: the pooling layer can extract grid attributes that are not disturbed by spatial location, improve the sensory field of subsequent features, and enable the network to obtain global information: in addition, the pooling layer can also realize the downsampling of the output of the convolutional layer, reduce the dimension of the intermediate hidden layer, and reduce the computational volume of the next layers while retaining important features.

The pooling layer generally uses maximum pooling or average pooling, and the average pooling used in this paper can be formulated as:

$$X^l = X^{l-1} \otimes P^l \tag{2}$$

In the formula, each element of the pooling kernel $P^l \in \square^{C\times H\times W}$ has a value of $1/(H\times W)$.

(3) Activation layer: the activation layer is able to introduce nonlinear factors to realize the mapping to the high-dimensional nonlinear space and further enhance the expressive ability of the network. Considering the non-negative number of grid faults predicted by the model, the specific activation function is set to be ReLU. it can accelerate the model convergence and enhance the sparse representation of the neural network at the same time:

$$ReLU(x) = \max(x, 0) \tag{3}$$

II. A. 2) LSTM networks

LSTM is a special type of recurrent neural network (RNN) specifically designed to process temporal data. Compared to standard RNNs, LSTMs not only share parameters through input temporal sequences, but also have advantages in long sequence processing and gradient vanishing problems.As a temporal model, LSTMs have the ability to efficiently capture both long- and short-term temporal dependencies in sequences through the introduction of a gating mechanism, which can be used to satisfy temporal prediction tasks at different scales.

The core idea of the LSTM network is the introduction of an internal memory unit called a cell, which retains the information in the input sequence over long time intervals and controls the input and output of the information. The memory of the LSTM network for the sequence is kept in the cell, which is also regulated by the input gate i_t and the forgetting gate f_t. In each time step, the LSTM network calculates the cell state and output of the current moment and passes them to the next moment based on the inputs, the output of the previous moment, and the cell state of the previous moment, which are weighted and summed and controlled by some gating mechanisms, including the input gate i_t, the forgetting gate f_{iota} and the output value of the output gate o_t :

$$i_t = \sigma(W_i[h_{t-1}, x_t] + b_i) \tag{4}$$

$$f_t = \sigma(W_f[h_{t-1}, x_t] + b_f) \tag{5}$$

$$g_t = \tanh(W_g[h_{t-1}, x_t] + b_g) \tag{6}$$

$$o_t = \sigma(W_o[h_{t-1}, x_t] + b_o) \tag{7}$$

$$c_t = f_t \square c_{t-1} + i_t \square g_t \tag{8}$$

$$h_t = o_t \square \tanh(c_t) \tag{9}$$

where W_f, W_i, W_o are the weight matrices of the oblivion gate, the input gate, and the output gate, respectively; W_g is the weight matrix used to compute the new cell state; b_f, b_i, b_o and $x\ b_f, b_i, b_o$ are the bias vectors for the forgetting gate, the input gate, the output gate, and the new cell state, respectively; $[h_{t-1}, x_t]$ denotes the vector that splices together the output of the previous timestep, h_{t-1}, and the input of the current timestep, x_t ; g_t and c_t are the candidate cell states and the cell state at the current moment, respectively; h_t is the final output of the LSTM; $\square$ is the Hadamard product; σ and tanh are the sigmoid and tanh activation functions, respectively:

$$\sigma(x) = \frac{1}{1+e^{-x}} \tag{10}$$

$$\tanh(x) = \frac{e^{x} - e^{-x}}{e^{x} + e^{-x}} \tag{11}$$

II. A. 3) CNN-LSTM networks

CNN-LSTM networks [17], [18] enable the integration of spatial model CNNs and temporal model LSTMs into a unified framework, aiming at overcoming the limitations of the respective models, integrating the advantages of CNNs in spatial feature extraction and LSTMs in temporal dynamic modeling, which can capture information in different spatial scales and temporal scales, and make the models more adaptable to different complex data patterns. The data input to the CNN is relatively independent from the rest of the dimensions due to the batch size where the dimensions are located, and the CNN generally processes the rest of the dimensional data in parallel. Therefore, the input data format of CNN needs to expand the batch size into the product of timing length and batch size, and ensure a certain degree of ordering. The output of CNN is reshaped to separate the timing length as a separate dimension, forming the standard input format of LSTM, which is used as the input of LSTM, so that it can further learn the timing correlation relationship at a higher level.

II. B.CNN-LSTM model design based on battery current outputs

II. B. 1) Data pre-processing

The data are first pre-processed, and the data set is divided into training set and validation set according to the ratio of 9:1. In the data cleaning stage, each parameter is first analyzed and processed, including the processing of data outliers, missing values, and the standardization of data and other operations. When dealing with outliers, data with obvious abnormalities in certain parameters are first deleted; at the same time, data without yield are deleted to exclude the interference of human factors.

II. B. 2) Data normalization

Due to the different value ranges and different units of the collected feature data, the input and output data are processed in order to better train the model and achieve better convergence, excluding the influence of different dimensions between production indicators. In this paper, the data values are mapped to the interval [0, 1] using the normalization method with the normalization formula:

$$X = \frac{x - x_{\min}}{x_{\max} - x_{\min}} \tag{12}$$

where X is the normalized value, x is the eigenvalue of a production indicator, $x_{\min}$ is the minimum value of the production indicator, and $x_{\max}$ is the maximum value of the production indicator.

II. B. 3) Model Design and Algorithm Construction

The model first receives the data using a CNN and extracts spatial features related to temporal variables from the convolutional and pooling layers of the CNN. After data cleaning, the extracted features are passed to the LSTM layer to extract temporal features from the sequence data. Ultimately, based on the CNN-LSTM approach, the model can generate predictions of solar cell current output in the fully connected layer. The input of the model is the significant feature parameters extracted by the CNN, and the output is the solar cell output data.The CNN-LSTM model mainly consists of a CNN module and an LSTM module.The CNN module contains one convolutional layer with a convolutional kernel size of 3, a convolutional kernel number of 64, an activation function of ReLU, and one layer of maximal pooling, with a pooling layer size of 2. The LSTM module contains 128 nodes, and the random dropout rate (Dropout) of LSTM is 0.2. The loss function of the model uses MAE.

II. B. 4) Model Training Process

According to data preprocessing and model design and algorithm construction, the training process of the model can be obtained. First, the data are preprocessed to remove the missing values and outliers; subsequently, the data are normalized by algorithm adjustment to obtain the experimental data that will be input into the model. After that, the training of the model begins.

II. C.Nonlinear modeling of solar cell output characteristics

II. C. 1) Calculating the output factor of a solar cell

The shape factor from one differential area element dA_1 to another differential area element dA_2 in a solar cell can be expressed by dF_{d1-d2}, when the 2 area elements have the following relationship:

$$dE_{d_1-d_2} = \frac{\cos\theta_1 \cos\theta_2}{\pi S^2_{d_1-d_2}} dA_2 \tag{13}$$

Since the definition of each parameter can be converted to the case of a finite area of the solar surface, the output factor can then be expressed as:

$$E_{d_1-d_2} \frac{1}{A_1} \int_{A_1} \int_{A_2} \frac{\cos\theta_1 \cos\theta_2}{\pi S^2_{d_1-d_2}} dA_2 dA_1 \tag{14}$$

Based on the output factor, the equivalent circuit of the joint solar cell is used to calculate the solar cell output current. The output current is obtained as:

$$i_{pw} = I_{pn} - I_{rf}\left[\exp\frac{q}{AkT}(U + i_{pw}R_c) - 1\right] - \frac{U + i_{pw}R_c}{R_{cb}} \tag{15}$$

i_{pw} is the panel output current; I_{pn} is the photogenerated current; U is the external voltage of the solar cell; R_c is the series resistor; R_{cb} is the parallel resistor; I_{rf} is the reverse saturation current of the diode; k is the Boltzmann constant; q is the electronic charge; A is the diode characteristic factor in the solar cell; and T is the solar cell surface temperature.

II. C. 2) Determination of model parameters

Since the series resistance R_c has a very small value but the parallel resistance R_{cb} is extremely large and is known from the expression for the output characteristics of a solar cell in an ideal state:

$$i_{pw} = I_{pn} - I_{rf}\left[\exp\frac{q}{AkT} - 1\right] \tag{16}$$

Setting five parameters, the parameters of solar cell output characteristics can be expressed as follows according to the current and voltage corresponding to the maximum power output from the solar energy:

$$\begin{cases} i_{pw} = I_{sd}\left\{1 - C_1\left[C_1 \exp\dfrac{U}{C_2 Uc}\right]\right\} \\ C_1 = \left(1 - \dfrac{I_m}{I_{sd}}\right)\exp\left(-\dfrac{U_m}{C_2 Uc}\right) \\ C_2 = \dfrac{Uc}{\ln\dfrac{U_m}{C_2 Uc}} \end{cases} \tag{17}$$

where: U_m is the voltage out of the maximum power point; I_m is the current at the maximum point; Uc is the open-circuit voltage; and C_1C_2 is the characteristic coefficient. Due to the effect of temperature and light factor on the solar cell, the corrected output equation for voltage is calculated as:

$$\begin{cases} \Delta I = \alpha S \Delta\Gamma + (S-1) I_{sd} \\ \Delta V = -\beta \Delta T - R_c \Delta I \end{cases} \tag{18}$$

where: α is the current temperature correction coefficient of solar cell; β is the correction coefficient of voltage temperature. Transform Eq. (18) and substitute it into Eq. (17) to finally obtain 4 model parameters, solar cell output voltage V, output current I, and start-up gap S_1, instantaneous ambient temperature T_1. Based on the parameters of the above four models, the nonlinear modeling of the current output characteristics of solar cells is finally completed.

II. C. 3) Completion of nonlinear modeling

The four parameters obtained above are described using the method of harmonic analysis [19]. The initial nonlinear link of the solar cell output characteristics can be expressed as:

$$y = f(x) \tag{19}$$

When the output of a nonlinear link behaves as a sinusoidal output, it can be expressed as:

$$x(t) = B \sin \omega t \tag{20}$$

At this point, the nonlinear link of the solar cell is at steady state output, and the ratio of the harmonic component to the output voltage is the model descriptive function of the final solar cell output characteristics, which can be expressed as:

$$M(A) = \frac{I}{A} V e^{S_1} \tag{21}$$

From the above equation, it can be seen that the output characteristic $f(x)$ of the nonlinear model should be an odd function, and the sinusoidal output condition of t can ensure that the mathematical model of the solar cell output characteristic does not contain a constant value component, keeping the rigor of the final model, and in summary, the final completion of the nonlinear modeling of the output characteristic of the solar cell.

III. Analysis of the results of environmental sensitivity tests on the current output of solar cells

III. A. CNN-LSTM based solar cell current prediction

III. A. 1) Prediction of battery current output by different models

This section analyzes the experimental results of solar cell current output power prediction based on LSTM and CNN-LSTM neural networks. This experiment uses solar cell current output power generation data from a region in the northern hemisphere, and mainly considers four important factors that affect the solar cell current output power: solar radiance, air temperature, air pressure and humidity. We compare the prediction effect of the two models in the training set and the test set by four evaluation indexes, RMSE, MAE, MAPE and R^2.The prediction effect values of the two models in the training set and the test set are shown in Table 1. From the table, it can be seen that the prediction performance of the CNN-LSTM model is better than that of the single LSTM model on both the training set and the test set. On the training set, the RMSE of CNN-LSTM decreases from 1.0619 to 0.9042 for LSTM, MAE

decreases from 0.7834 to 0.6401, MAPE decreases by 0.1485 percentage points, and the R^2 improves from 0.9732 to 0.9928.

This shows that the CNN-LSTM model is more accurate in fitting known data and is better able to capture the trend of solar cell current output power. On the test set, the advantage of the CNN-LSTM model is even more obvious. The RMSE of CNN-LSTM is reduced from 1.6771 to 1.1586 for LSTM, and the MAPE is also reduced from 11.099% to 5.605%, and the R^2 is improved from 0.9096 to 0.9761. It can be seen that CNN-LSTM shows stronger generalization ability and significantly less prediction error in the face of unknown data, indicating that the model can better deal with the influence of external environmental variables.

Table 1: The prediction of two models of training set and test concentration

Model	Data set	RMSE	MAE	MAPE(%)	R^2
LSTM	Training set	1.0619	0.7834	6.175	0.9732
LSTM	Test set	1.6771	0.9959	11.099	0.9096
CNN-LSTM	Training set	0.9042	0.6401	4.529	0.9928
CNN-LSTM	Test set	1.1586	0.9868	5.605	0.9761

III. A. 2) Accuracy of CNN-LSTM model prediction results

The neural network prediction results in the training and test sets are shown in Fig. 1, where (a) and (b) represent the training and test sets, respectively. Through our further analysis of the model's prediction results, it can be seen from the comparison of the training set that the prediction curves of the CNN-LSTM model are highly overlapped with the actual values, while the prediction curves of the LSTM have some deviation from the actual values, especially at some local peaks. The CNN-LSTM model utilizes the local features extracted from the convolutional layer to accurately capture the small fluctuations in the solar cell current output power as a function of the environment. From the comparison of the test sets, it can be seen that although the prediction accuracies of both models have decreased, CNN-LSTM still significantly outperforms the LSTM model, and CNN-LSTM can more accurately capture the trend inflection points in the complex fluctuation intervals. Taken together, the model shows stronger robustness and generalization ability in solar cell current output power prediction.

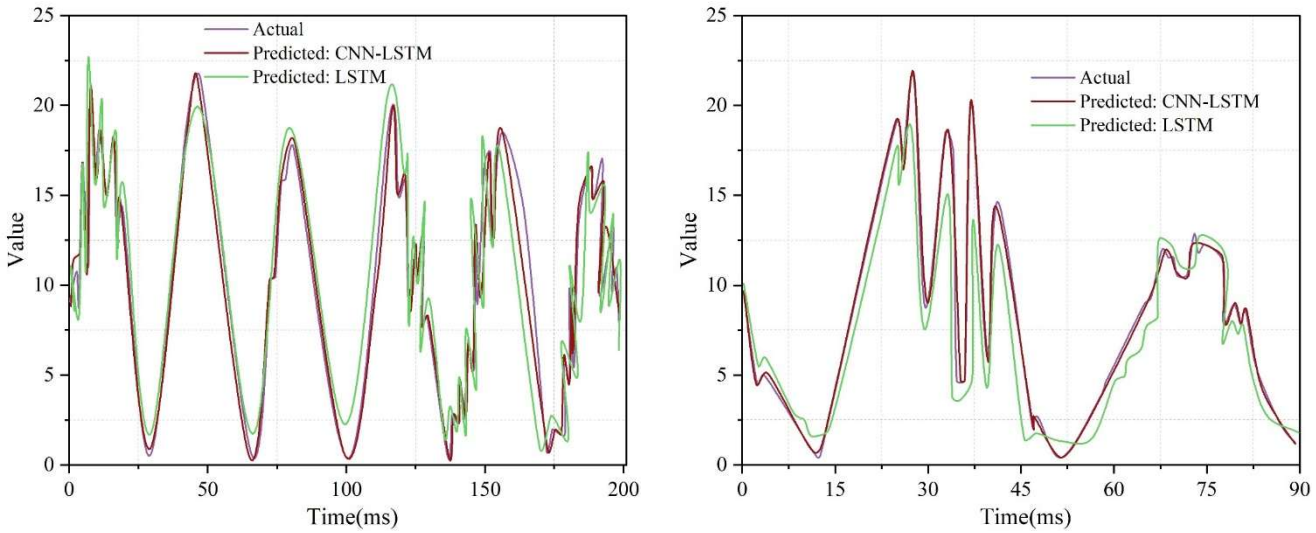

(a)Training set (b)Test set

Figure 1: The training set and the test focus neural network forecast results

III. B. Research on the environmental sensitivity of solar cells

III. B. 1) Sensitivity of solar cells to relative humidity

After the same treatment, five types of solar cells with different thicknesses of insulating film were tested at T=28°C and RH=99% to determine the relationship between the corrosion current and the thickness of insulating film to analyze how the thickness of the insulating film affects the sensitivity of the cells to relative humidity. The relationship between insulation film thickness and solar cell current is shown in Figure 2. Nonlinear fitting of the test data yields

$I_g = 6.76147\exp(-d/0.24011)$, and the square of the correlation coefficient is $R^2 = 0.99965$, where I_g is the corrosion current, μA; and d is the thickness of the insulating film, mm.

The results of this test show that the corrosion current decays exponentially with the increase of the insulating film thickness, i.e., the sensitivity of the corrosion cell to the relative humidity when it is not covered with a visible liquid film decreases exponentially with the increase of the insulating film thickness.

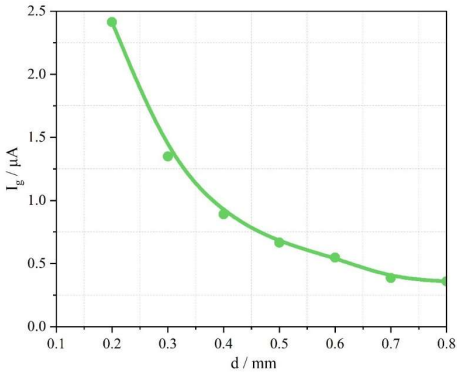

Figure 2: The relationship between insulation membrane and battery current

III. B. 2) Solar cell response to relative humidity

Keeping the temperature constant at 18, 26, 38 and 46°C to study the response of the cell corrosion current I_g to the change of RH, the effect of RH on the corrosion current of the solar cell at different temperatures is shown in Fig. 3.

After fitting analysis, the relationship equation between RH and corrosion current at different temperatures satisfies $\lg I_g = A + B \cdot RH$ (A and B are constants). The specific relational equations at different temperatures are as follows (where R is the correlation coefficient):

$$T = 18℃, \lg I_g = -1.71321 + 0.01369RH, R = 0.97941$$

$$T = 26℃, \lg I_g = -1.560134 + 0.0121RH, R = 0.98019$$

$$T = 38℃, \lg I_g = -1.29141 + 0.01208RH, R = 0.99617$$

$$T = 46℃, \lg I_g = -1.22954 + 0.014312RH, R = 0.99572$$

This indicates that the logarithm of RH and corrosion current are linearly related when the temperature is constant, which on the other hand proves that the solar cell current can reflect the change of RH in a timely manner. In addition, with the increase of temperature, the curve of the relationship between RH and corrosion current shifts upward and basically remains parallel, i.e., the higher the temperature, the greater the corrosion rate for a certain humidity.

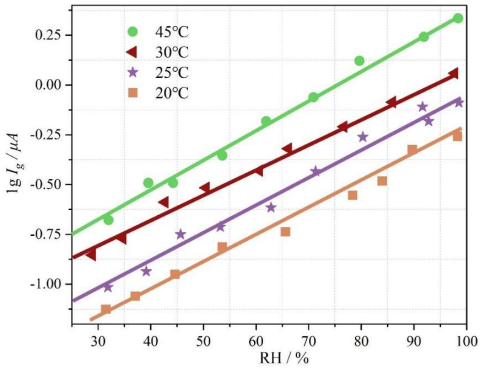

Figure 3: The effect of relative humidity on the current at different temperatures

III. B. 3) Solar cell response to temperature

The relative humidity was kept constant at 25%, 50%, 75%, 85% and 100% to study the response of the cell corrosion current I_g to the temperature change, and the effect of temperature on the corrosion current of the solar cell at different relative humidities is shown in Fig. 4.

After fitting and analyzing the relationship between temperature T and corrosion current under different humidity is derived to satisfy the form of $\lg I_g = C + D \cdot T$ (C, D is a constant), and its specific expression under different humidity is:

$$RH = 25\%, \lg I_g = -1.60743 + 0.02105T, R = 0.95879$$

$$RH = 50\%, \lg I_g = -1.21426 + 0.0177T, R = 0.9315$$

$$RH = 75\%, \lg I_g = -1.08241 + 0.02409T, R = 0.96521$$

$$RH = 75\%, \lg I_g = -0.79316 + 0.02243\,T, R = 0.98941$$

$$RH = 100\%, \lg I_g = -0.65843 + 0.02207\,T, R = 0.9948$$

The test results show that: at constant RH, the temperature and the logarithm of the solar cell corrosion current also show a linear relationship; with the rise of RH, the linear intercept increases and all the straight lines basically show a parallel state, i.e., the higher the temperature is, the higher the humidity is, the greater the corrosion rate is.

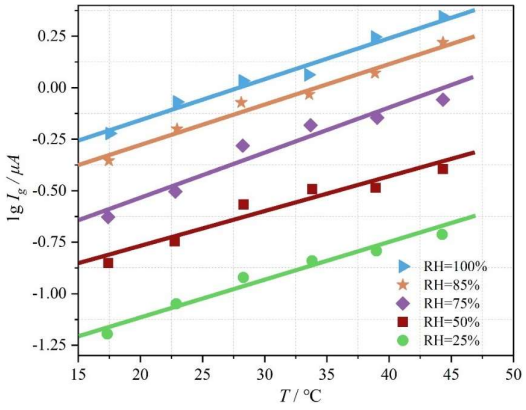

Figure 4: The effect of temperature on current in different relative humidity

IV. Conclusion

In this paper, we propose a hybrid model combining a convolutional neural network and a long-short-term memory network to improve the prediction accuracy of the model for solar cell current output and its sensitivity to environmental changes by extracting spatial features through the CNN and capturing long-term dependencies in the time series through the LSTM.

(1) The CNN-LSTM model outperforms the single LSTM model in all the metrics in the training and test sets. Incorporating multivariate features such as solar radiation, temperature, barometric pressure, and humidity significantly improves the prediction accuracy of the fluctuation trend of solar cell current output power. This paper also provides an effective solution for the intelligent management of solar cell current output power generation system in the future.

(2) The thickness of the insulating film affects the reliability and sensitivity of solar cells, of which 0.2mm and 0.8mm thick cells have better reliability and stability. The relationship between solar cell corrosion current and relative humidity and temperature follows the form: $\lg I_g = A + B \cdot RH$ and $\lg I_g = C + D \cdot T$, respectively. The solar cell has a good sensitivity to temperature and relative humidity.

References

[1] Yuan, K., Zhang, T., Xie, X., Du, S., Xue, X., Abdul-Manan, A. F., & Huang, Z. (2023). Exploration of low-cost green transition opportunities for China's power system under dual carbon goals. Journal of Cleaner Production, 414, 137590.

[2] Liu, L., Wang, Q., Lin, H., Li, H., & Sun, Q. (2017). Power generation efficiency and prospects of floating photovoltaic systems. Energy Procedia, 105, 1136-1142.

[3] Afkar, M., Gavagsaz-Ghoachani, R., Phattanasak, M., Martin, J. P., & Pierfederici, S. (2021). Proposed system based on a three-level boost converter to mitigate voltage imbalance in photovoltaic power generation systems. IEEE Transactions on Power Electronics, 37(2), 2264-2282.
[4] Yang, F., Sun, Q., Han, Q. L., & Wu, Z. (2016). Cooperative model predictive control for distributed photovoltaic power generation systems. IEEE Journal of Emerging and Selected Topics in Power Electronics, 4(2), 414-420.
[5] KR, C. L., Rajalakshmi, K., Simon, S., & Stepha, G. (2023, March). Impact of Shadow or Dust on Solar Photovoltaic Power Generation System. In 2023 Second International Conference on Electronics and Renewable Systems (ICEARS) (pp. 196-200). IEEE.
[6] Mustafa, R. J., Gomaa, M. R., Al-Dhaifallah, M., & Rezk, H. (2020). Environmental impacts on the performance of solar photovoltaic systems. Sustainability, 12(2), 608.
[7] Leccisi, E., Raugei, M., & Fthenakis, V. (2016). The energy and environmental performance of ground-mounted photovoltaic systems—a timely update. Energies, 9(8), 622.
[8] Tawalbeh, M., Al-Othman, A., Kafiah, F., Abdelsalam, E., Almomani, F., & Alkasrawi, M. (2021). Environmental impacts of solar photovoltaic systems: A critical review of recent progress and future outlook. Science of The Total Environment, 759, 143528.
[9] Saleem, A., Iqbal, A., Hayat, M. A., Panjwani, M. K., Mangi, F. H., & Larik, R. M. (2020). The effect of environmental changes on the efficiency of the PV system. Indonesian Journal of Electrical Engineering and Computer Science, 18(1), 558-564.
[10] Njok, A. O., Ogbulezie, J. C., & Akonjom, N. A. (2022). Evaluation of the performance of photovoltaic system under different wavelengths from artificial light in a controlled environment. Journal of Applied Sciences and Environmental Management, 26(6), 1015-1020.
[11] Renno, C., Petito, F., Landi, G., & Neitzert, H. C. (2017). Experimental characterization of a concentrating photovoltaic system varying the light concentration. Energy Conversion and Management, 138, 119-130.
[12] Iqbal, S., Khan, S. N., Sajid, M., Khan, J., Ayaz, Y., & Waqas, A. (2023). Impact and performance efficiency analysis of grid-tied solar photovoltaic system based on installation site environmental factors. Energy & Environment, 34(7), 2343-2363.
[13] Zatsarinnaya, J. N., Amirov, D. I., & Zemskova, L. V. (2019, June). Analysis of the environmental factors influence on the efficiency of photovoltaic systems. In IOP Conference Series: Materials Science and Engineering (Vol. 552, No. 1, p. 012033). IOP Publishing.
[14] Farooq, U., Mushtaq, M. F., Ullah, Z., Ejaz, M. T., Akram, U., & Aslam, S. (2025). Time Series Analysis of Solar Power Generation Based on Machine Learning for Efficient Monitoring. Engineering Reports, 7(2), e70023.
[15] Yang, D., Dong, Z., Lim, L. H. I., & Liu, L. (2017). Analyzing big time series data in solar engineering using features and PCA. Solar Energy, 153, 317-328.
[16] Shireen, T., Shao, C., Wang, H., Li, J., Zhang, X., & Li, M. (2018). Iterative multi-task learning for time-series modeling of solar panel PV outputs. Applied energy, 212, 654-662.
[17] Neeti Sangwan & Vishal Bhatnagar. (2025). Multi-branch LSTM encoded latent features with CNN-LSTM for Youtube popularity prediction.. Scientific reports,15(1),2508.
[18] Samanthisvaran Jayaraman & Anand Mahendran. (2025). CNN-LSTM based emotion recognition using Chebyshev moment and K-fold validation with multi-library SVM.. PloS one,20(4),e0320058.
[19] Xin Song,Xianglong Zhang,Wang Tian & Qiqi Zhu. (2025). TFMSNet: A time series forecasting framework with time–frequency analysis and multi-scale processing. Computers and Electrical Engineering,123(PD),110260-110260.